Electronic Supplementary Material (ESI) for Dalton Transactions.

# Electronic Supplementary Information

# Coordination chemistry of [2+2] Schiff-base macrocycles derived from the dianiline [(2-$NH_2C_6H_4)_2X$] (X = $CH_2CH_2$, O): Structural studies and the ROP capability towards cyclic esters.

Kuiyuan Wang,[a] Timothy J. Prior,[a] David L. Hughes,[b] Abdessamad Arbaoui ,[b] and Carl Redshaw [a*]

[a] *Department of Chemistry, University of Hull, HU6 7RX, U.K.*

[b] *School of Chemistry, University of East Anglia, Norwich, NR4 7TJ, U.K.*

**Contents**

**Figure S11**. Plot of ln $[CL]_0/[CL]_t$ *vs*. time using Fe complexes.

**Figure S12**. MALDI-ToF mass spectrum positive method for co-poly (ε-CL+ *r*-LA) (run 5).

**Figure S13**. MALDI-ToF mass negative method spectrum for co-poly (ε-CL+ *r*-LA) (run 5).

**Figure S14**. $^1$H NMR spectrum for co-poly (ε-CL+ *r*-LA) (run 5).

**Figure S15**. Gel permeation chromatography for co-poly (ε-CL+ *r*-LA) (run 5).

**Figure S16**. Plot (log Mw) of co-poly (ε-CL+ *r*-LA) (run 5).

**Figure S17**. $^{13}$C NMR spectrum for co-poly (ε-CL+ *r*-LA) (run 5).

**Figure S18**. 2D J-Resolved $^1$H NMR for co-poly (ε-CL+ *r*-LA) (run 5).

**Figure S19**. Plot of ln $[VL]_0/[VL]_t$ *vs*. time using Fe complexes.

**Figure S20**. $^1$H NMR (400 MHz, $CDCl_3$) spectrum for polyvaleroactone (run 4).

**Figure S21**. MALDI-ToF mass spectrum for polyvaleroactone (run 4).

**Figure S22**. $M_w$ *vs* number of δ-VL repeat units (n) afforded a straight line with a slope of 100.6 and an intercept of 131; the slope corresponds to the exact mass of the δ-VL monomer, whereas the intercept corresponds to a polymer chain structure with benzyloxy chain-ends plus $Na^+$ (δ-VL run 4).

**Figure S23**. 2D J-Resolved $^1$H NMR spectrum for co-poly (δ-VL+*r*-LA) (run 7).

**Figure S24**. $^1$H NMR spectrum for co-poly (δ-VL+*r*-LA) (run 7).

**Figure S25**. $^{13}$C NMR spectrum for co-poly (δ-VL+*r*-LA) (run 7).

**Figure S26**. MALDI-ToF mass spectrum for co-poly (δ-VL+*r*-LA) (run 7).

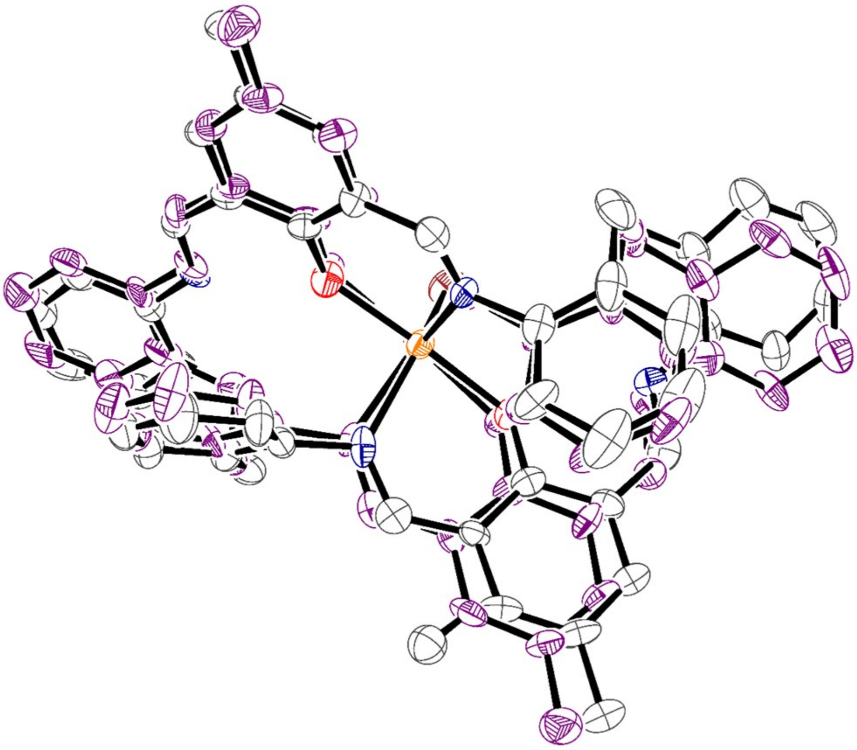

**Figure S1**. Different view showing the components of the structure (**1**·2MeCN).

There are two symmetry independent macrocyclic metal complexes in **1**·2MeCN. These are related by a pseudosymmetric translation of c/2. There is no evidence in the diffraction data that this is a strict symmetry element; the reflections with l odd have a mean intensity significantly different from zero and the refinement is stable using all reflections without the need for restraints.

It is possible to overlay the two parts of the structure (as shown above) and this demonstrates the deviation from a strict symmetry element.

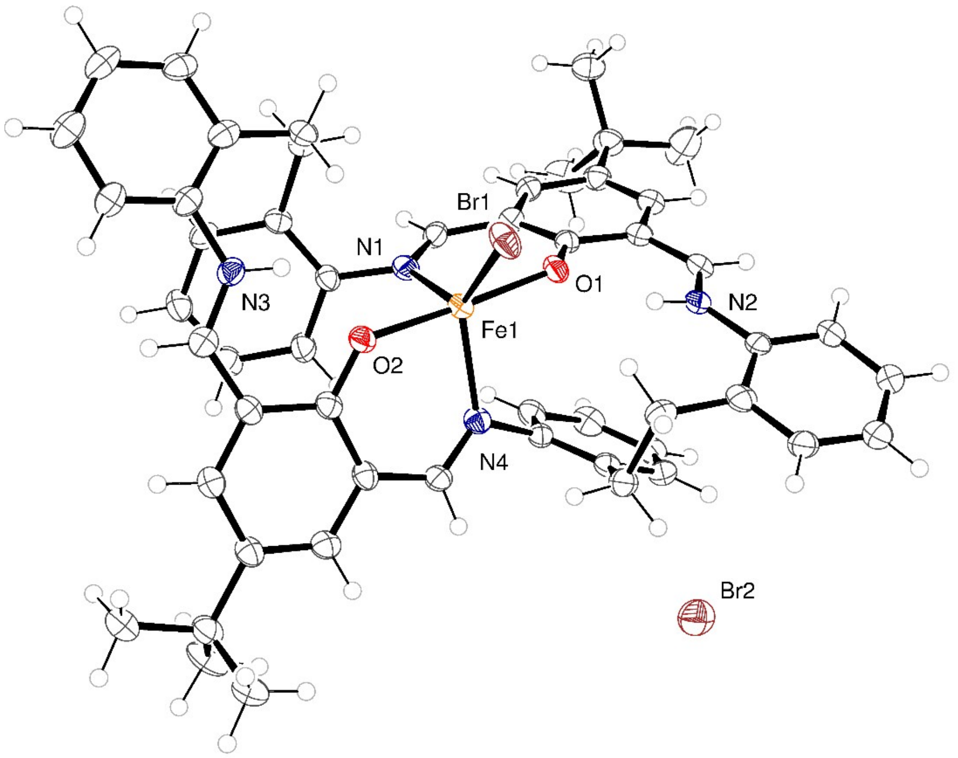

**Figure S2**. ORTEP plot of [FeBr($L^2H_2$)][Br] (**3**·5.5MeCN);

The structure **3** contains $Fe^{2+}$ which is five-coordinated in distorted tetrahedral geometry.

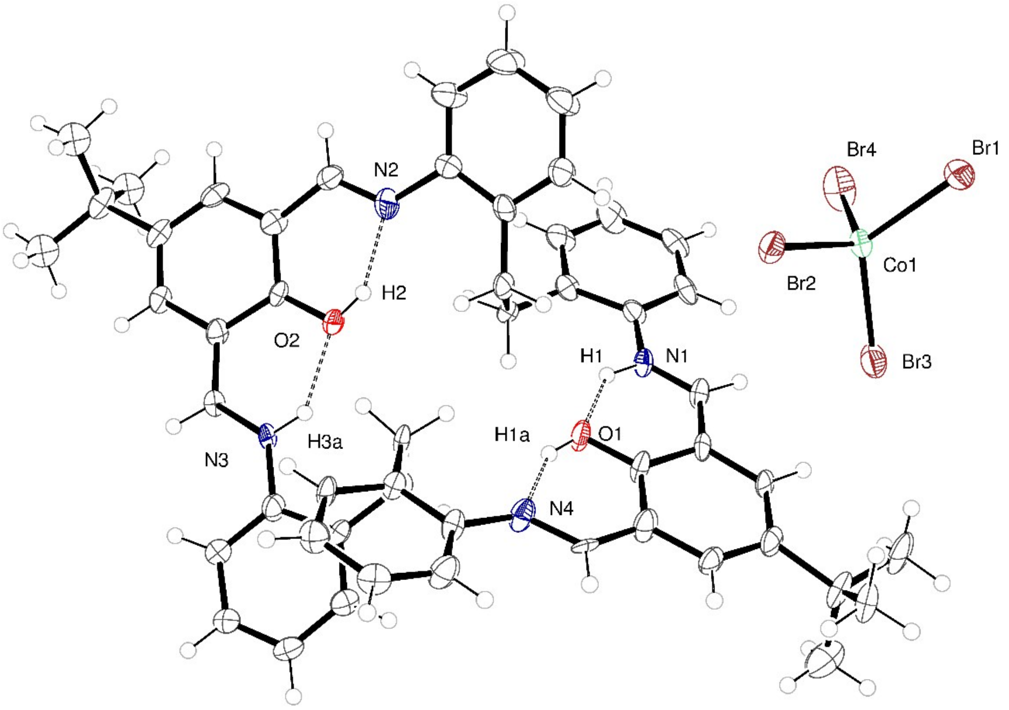

**Figure S3**. ORTEP plot of $[L_2H_2][CoBr_4]\cdot 2MeCN$ (**6**·2MeCN)

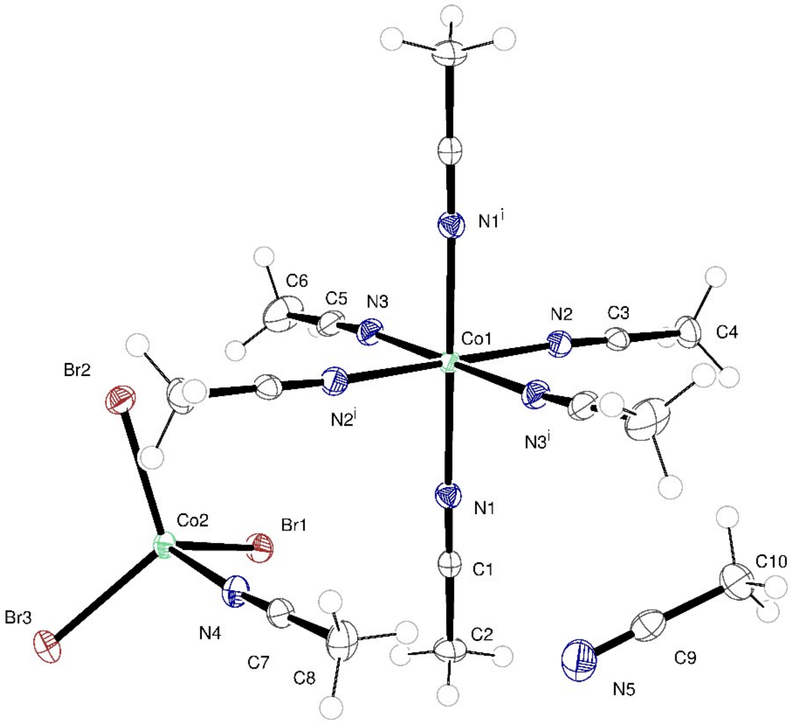

**Figure S4**. ORTEP plot of expanded asymmetric unit $[Co(NCMe)_6][CoBr_3NCMe]_2{\cdot}2MeCN$ (**9**·2MeCN); atoms labelled I are generated by the symmetry operator 4/3-x, 2/3-y, 2/3-z. Selected bond lengths (Å) and angles ($^{o}$): Co(1)–Br(1) 2.4874(12), Co(1)–O(11) 2.041(4), Co(1)–O(14) 2.009(4), Co(1)–N(37) 2.072(6), Co(1)–N(67) 2.081(6); O(11)–Co(1)–O(41) 176.64(19), N(37)–Co(1)–N(67) 110.3(2), O(11)–Co(1)–Br(1) 86.10(15).

The structure **10**·2MeCN contains $Co^{2+}$ in both octahedral and distorted tetrahedral geometry. The $[Co(NCMe)_6]^{2+}$ ion resides on an inversion centre and is a little distorted from a perfect octahedron despite the six identical ligands. $[CoBr_3NCMe]$ formally has $C_{3v}$ symmetry at the metal centre.

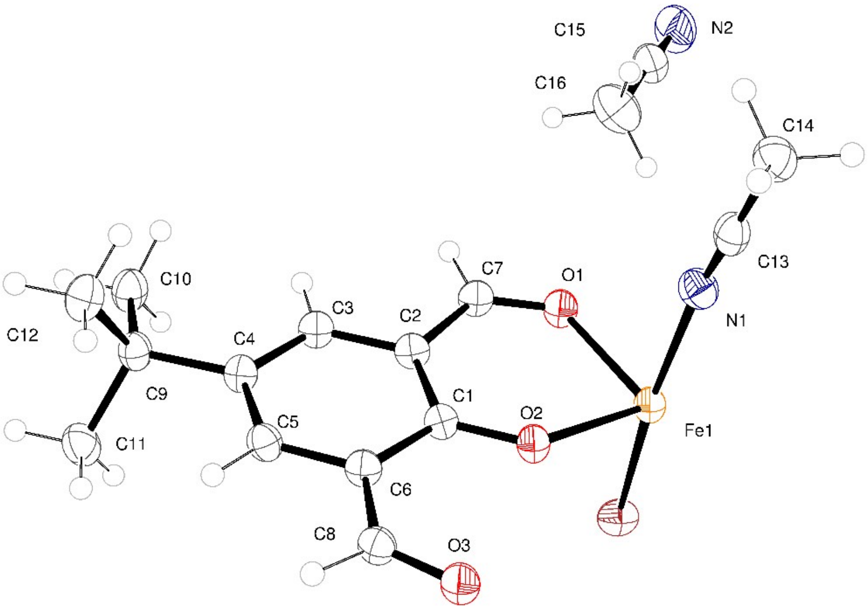

**Figure S5**. ORTEP plot of [FeBr(NCMe)$L_5$]$_2$·2MeCN (12·2MeCN) (**12**);

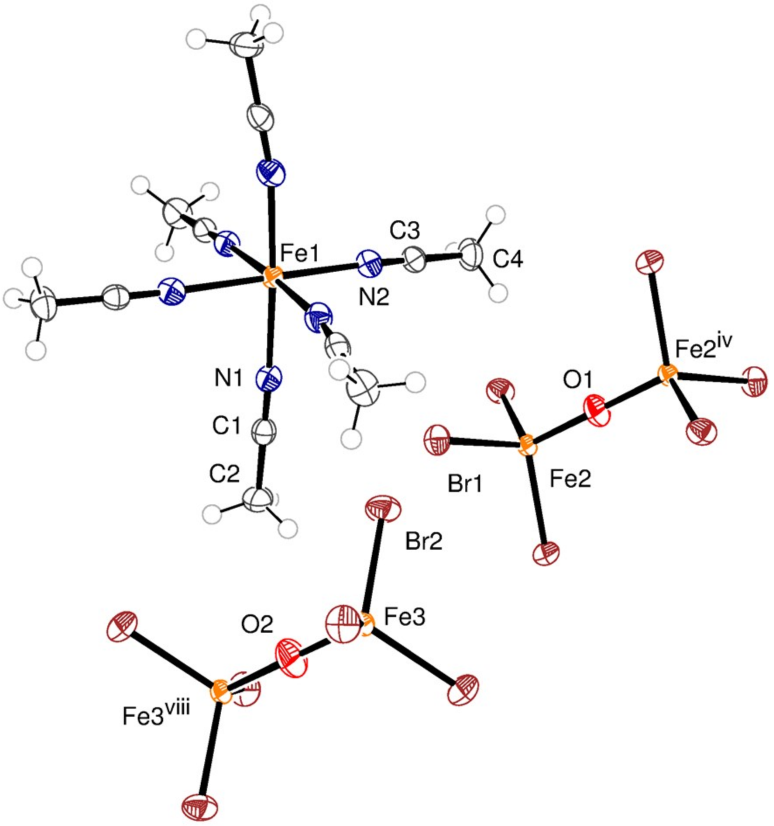

**Figure S6**. ORTEP plot of [Fe(NCMe)$_6$][FeBr$_3$OFeBr$_3$] (**13**); atoms labelled I are generated by the symmetry operator 2-x, 2-y, 1-z. Selected bond lengths (Å) and angles (°): Fe(1) – N(1) 2.159(2), Fe(1) – N(2) 2.162(2), Fe(1)–Br(1) 2.3634(3), Fe(2) – O(1) 1.7664(6), Fe(3) – O(2) 1.7625(6); N(1) – Fe(1) – N(2) 89.77(7).

As for structure **10**·2MeCN, the structure **13**·MeCN contains Fe$^{2+}$ in both octahedral and distorted tetrahedral geometry. The [Fe(NCMe)$_6$]$^{2+}$ ion resides on an inversion centre and is a little distorted from a perfect octahedron despite the six identical ligands.

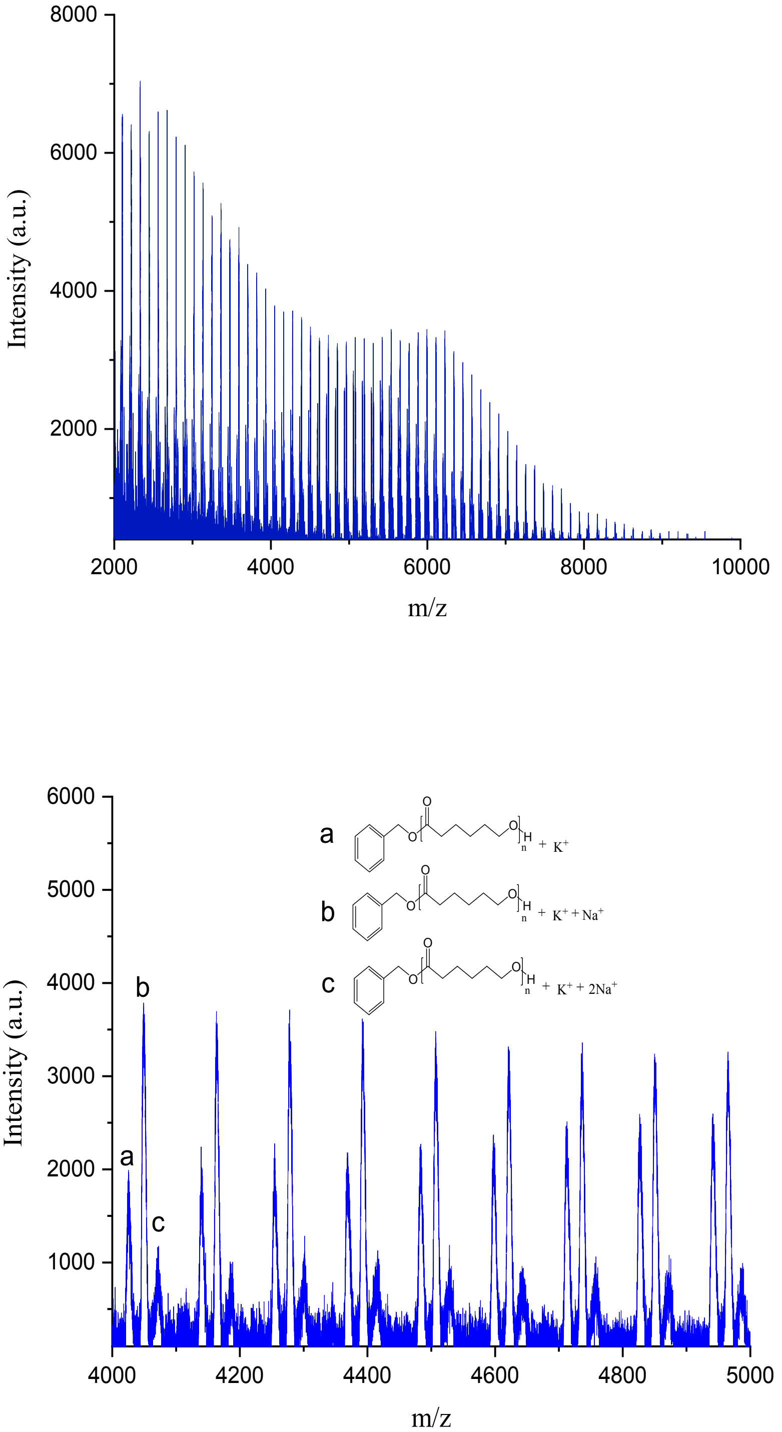

**Figure S7**. MALDI-ToF mass spectrum for polycaprolactone (run 5).

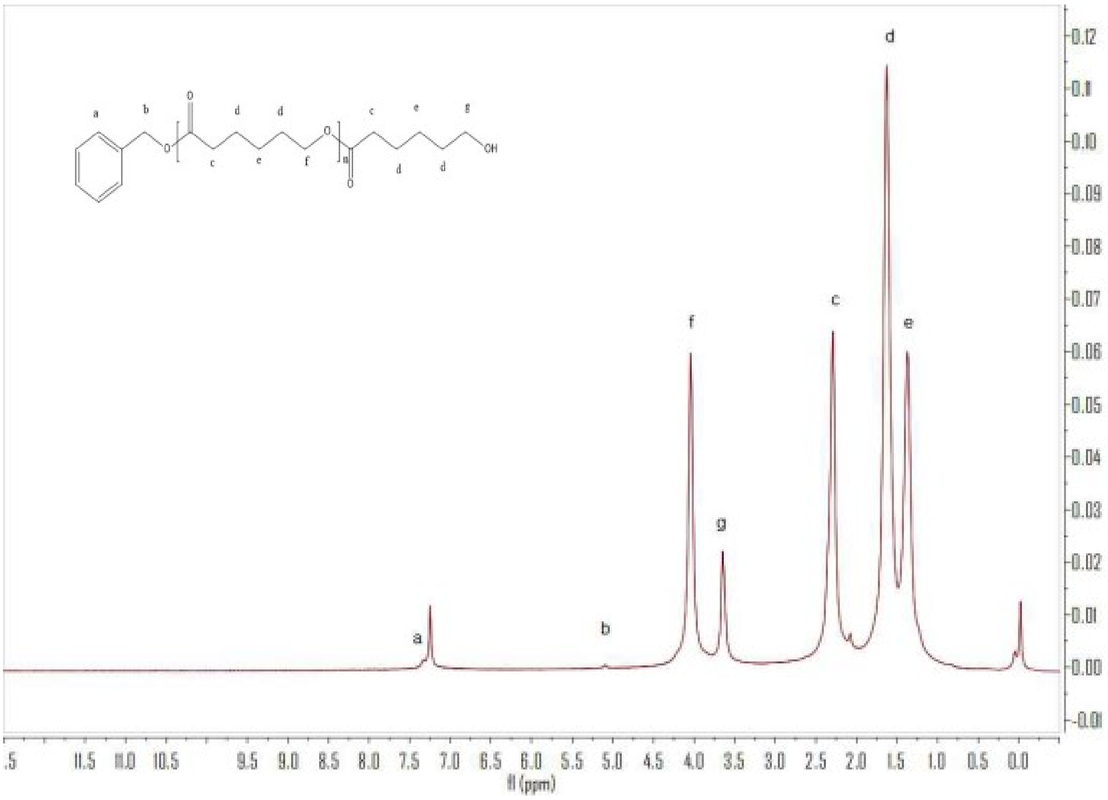

**Figure S8**. $^1$H NMR (400 MHz, $CDCl_3$) spectrum for polycaprolactone (run 5).

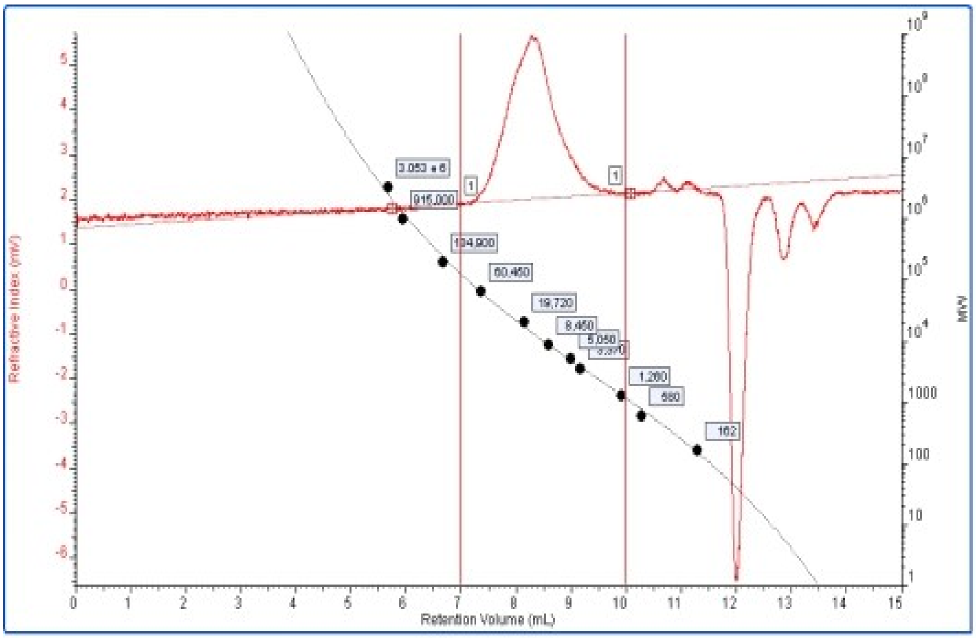

**Figure S9**. Gel permeation chromatography for polycaprolactone (run 5).

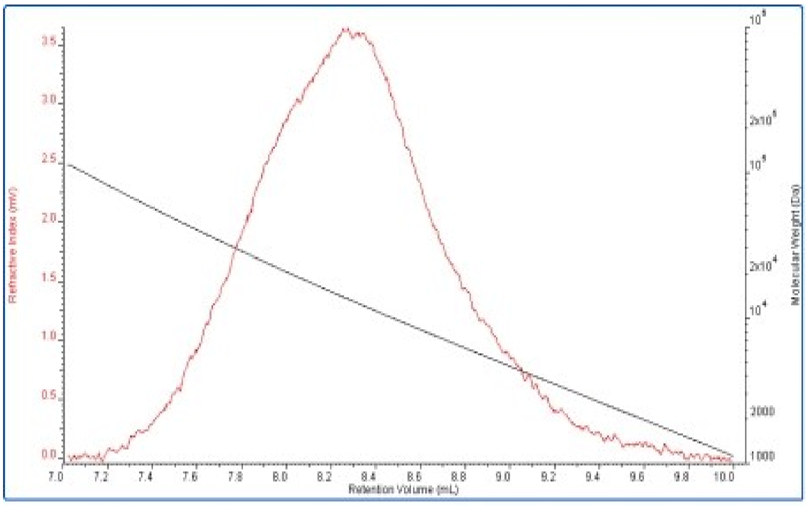

**Figure S10.** Plot (log $M_w$) of polycarbonate formed for polycaprolactone (run 5).

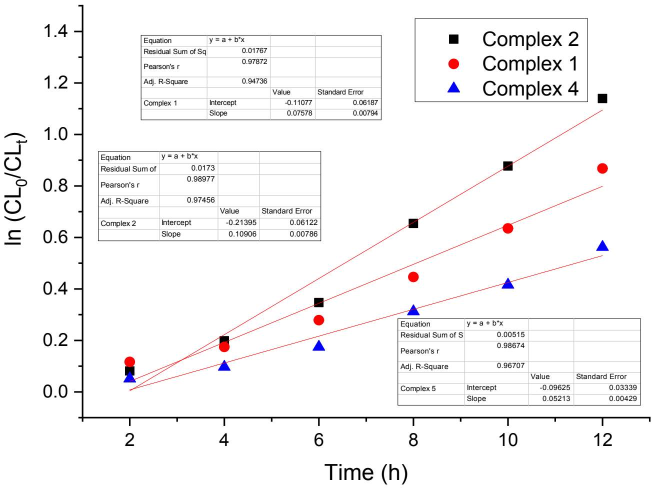

| Equation | y = a + b*x | | |
|---|---|---|---|
| Residual Sum of Sq | 0.01767 | | |
| Pearson's r | 0.97872 | | |
| Adj. R-Square | 0.94736 | | |
| | | Value | Standard Error |
| Complex 1 | Intercept | -0.11077 | 0.06187 |
| | Slope | 0.07578 | 0.00794 |

| Equation | y = a + b*x | | |
|---|---|---|---|
| Residual Sum of | 0.0173 | | |
| Pearson's r | 0.98977 | | |
| Adj. R-Square | 0.97456 | | |
| | | Value | Standard Error |
| Complex 2 | Intercept | -0.21395 | 0.06122 |
| | Slope | 0.10906 | 0.00786 |

| Equation | y = a + b*x | | |
|---|---|---|---|
| Residual Sum of S | 0.00515 | | |
| Pearson's r | 0.98674 | | |
| Adj. R-Square | 0.96707 | | |
| | | Value | Standard Error |
| Complex 5 | Intercept | -0.09625 | 0.03339 |
| | Slope | 0.05213 | 0.00429 |

**Figure S11**. Plot of ln $[CL]_0/[CL]_t$ *vs.* time using Fe complexes ([monomer]:[Cat]:BnOH=500:1:1; 130 °C).

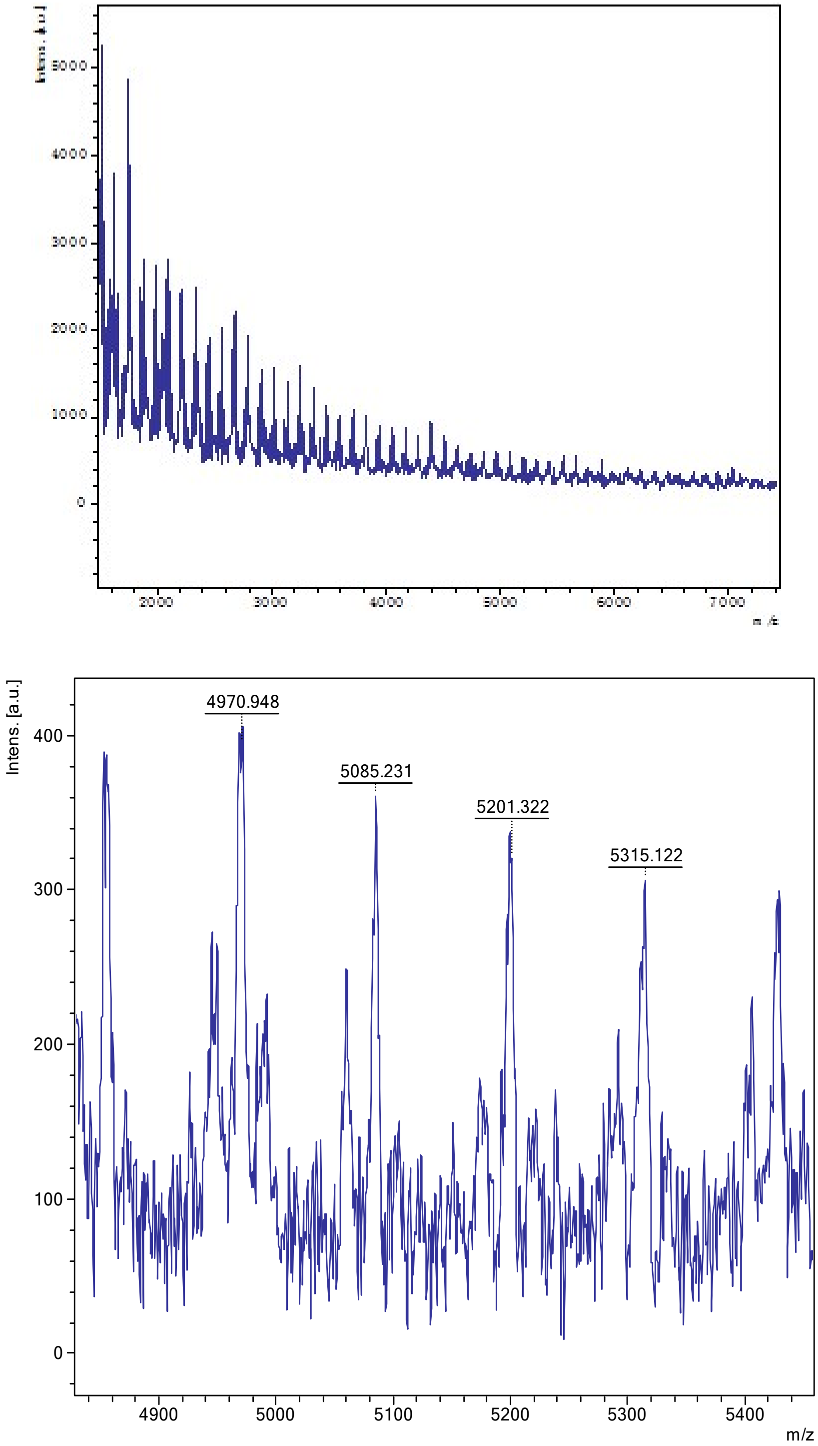

**Figure S12**. MALDI-ToF mass spectrum positive method for co-poly (ε-CL+ *r*-LA) (run 5).

The gap of 114 correspondes to the molecular weight of ε-CL.

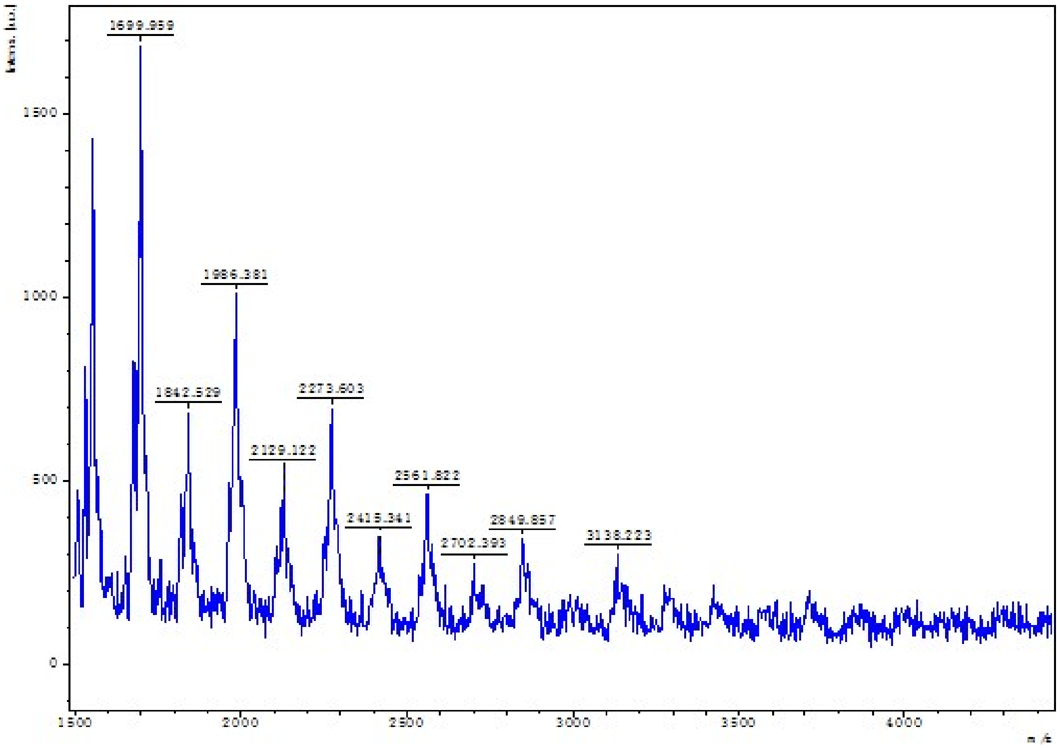

**Figure S13**. MALDI-ToF mass negative method spectrum for co-poly (ε-CL+ *r*-LA) (run 5).

The gap of 144 corresponds to the molecular weight of *r*-LA.

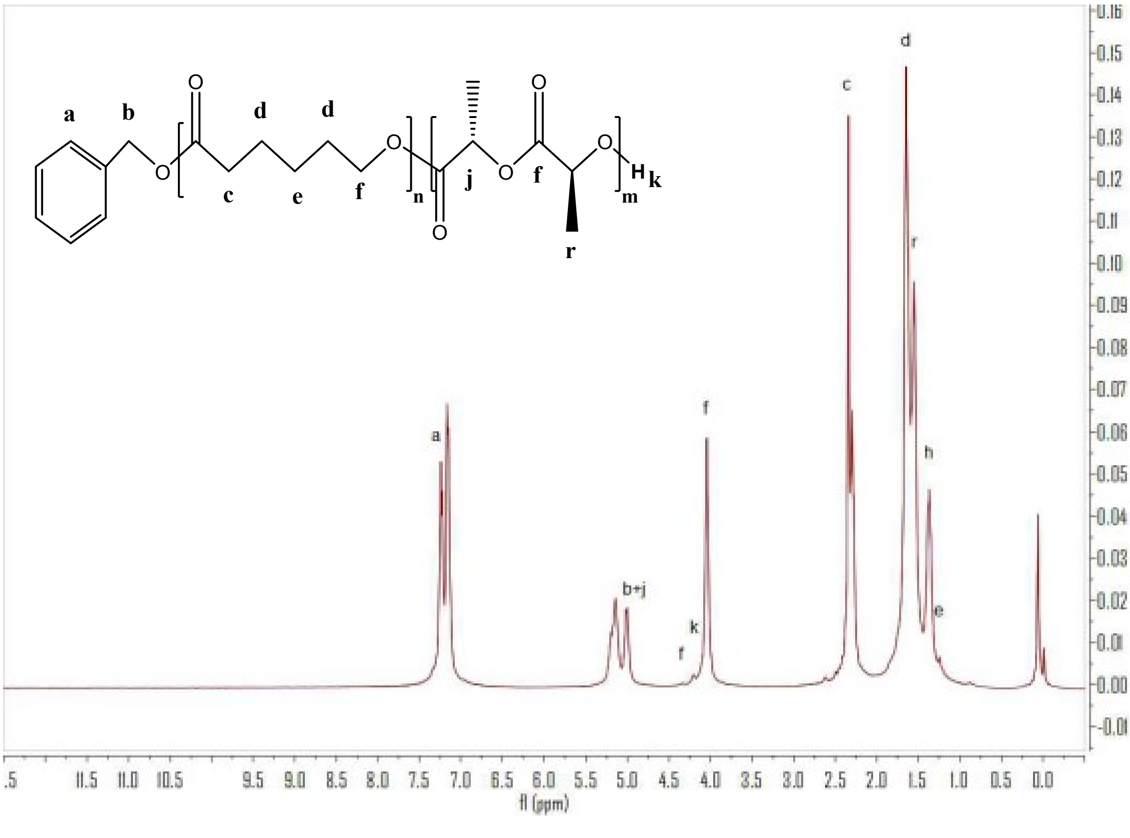

**Figure S14**. $^1$H NMR spectrum for co-poly (ε-CL+ *r*-LA) (run 5).

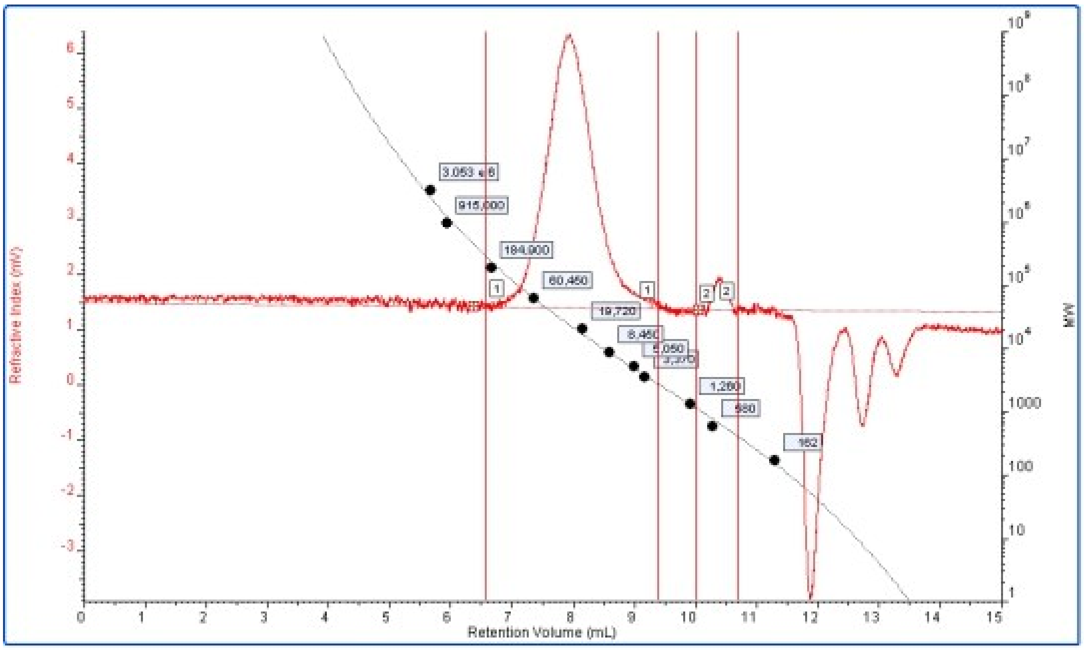

**Figure S15**. Gel permeation chromatography for co-poly (ε-CL+ *r*-LA) (run 5).

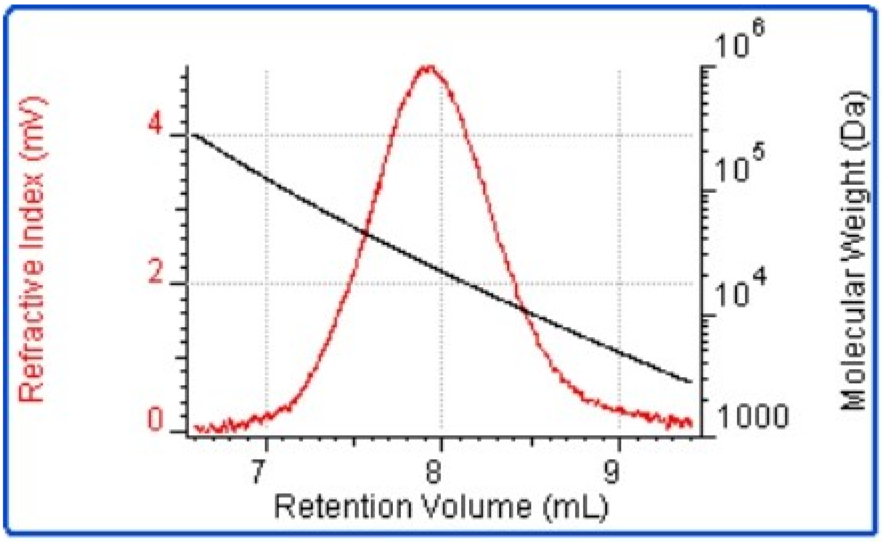

**Figure S16**. Plot (log $M_w$) of co-poly (ε-CL+ *r*-LA) (run 5).

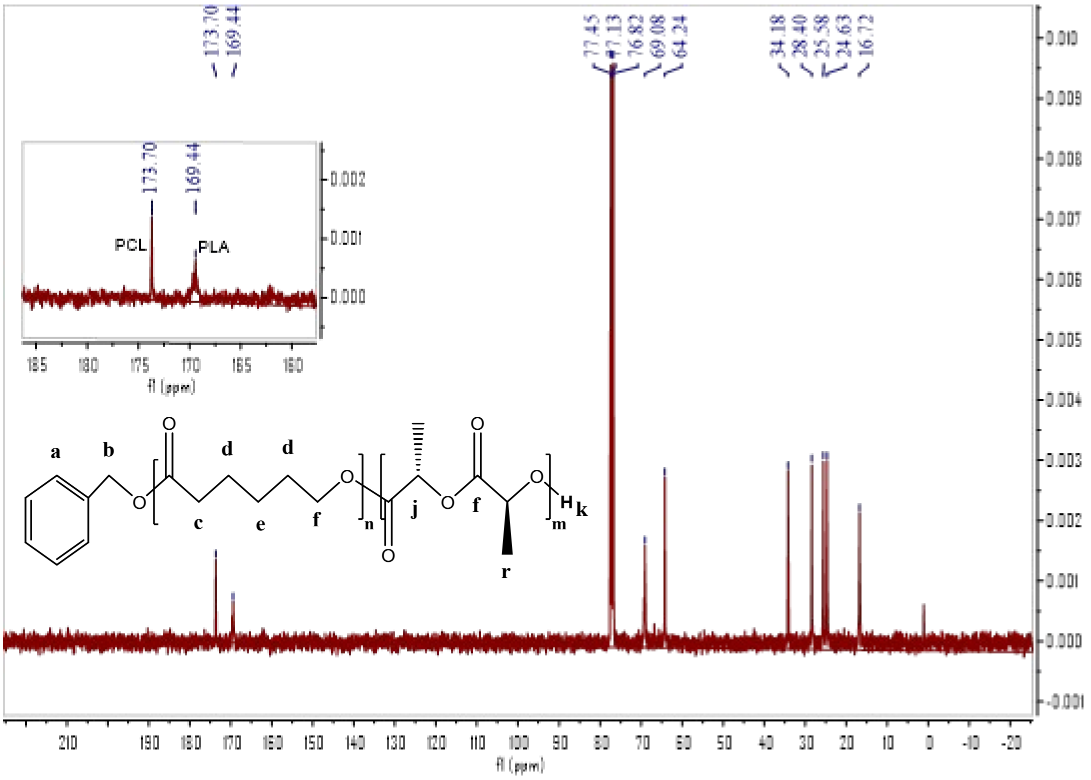

**Figure S17**. $^{13}$C NMR spectrum for co-poly (ε-CL+ *r*-LA) (run 5).

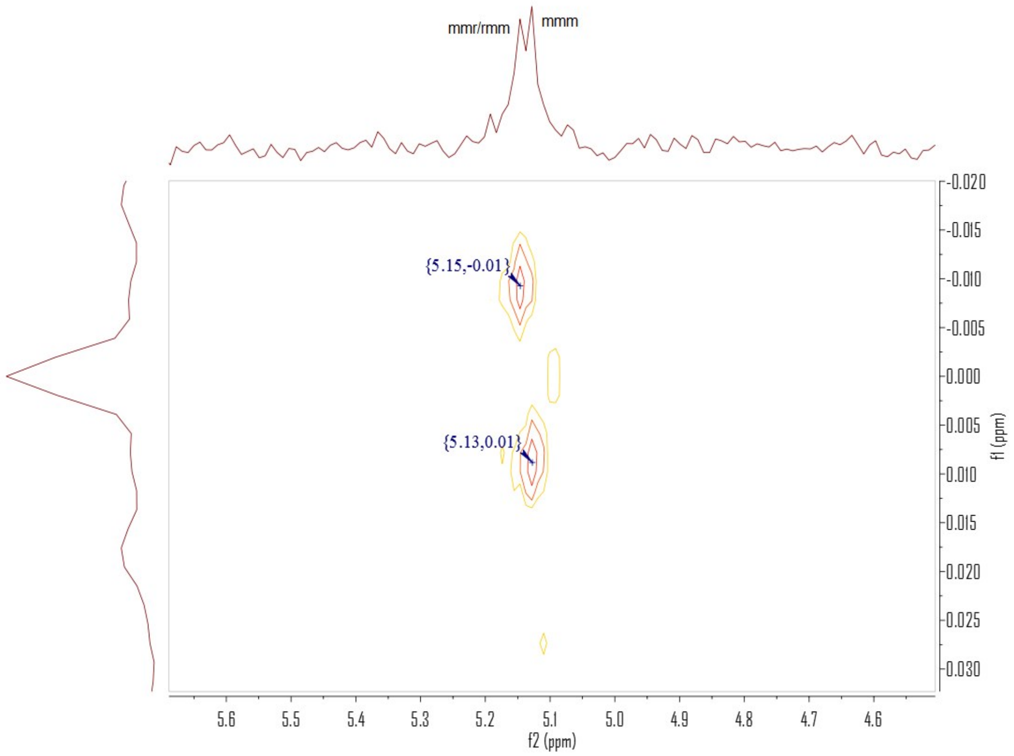

**Figure S18**. 2D J-Resolved $^1$H NMR spectrum for co-poly (ε-CL+ *r*-LA) (run 5).

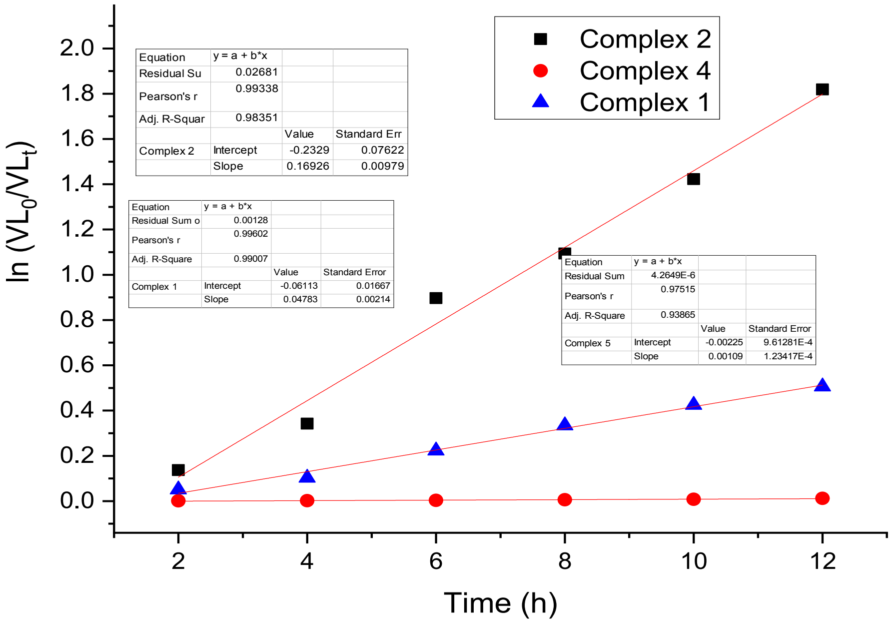

**Figure S19**. Plot of ln $[VL]_0/[VL]_t$ *vs.* time using Fe complexes ([monomer]:[Cat]:BnOH=500:1:1; 130 °C).

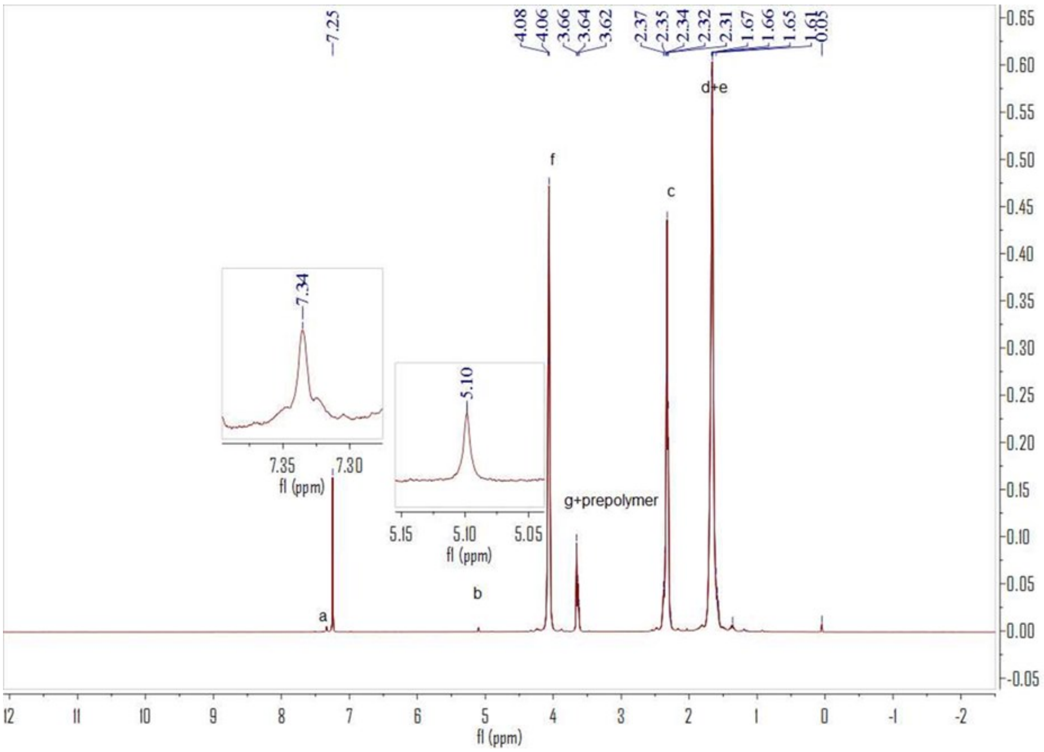

**Figure S20**. $^1$H NMR (400 MHz, $CDCl_3$) spectrum for polyvalerolactone (run 4).

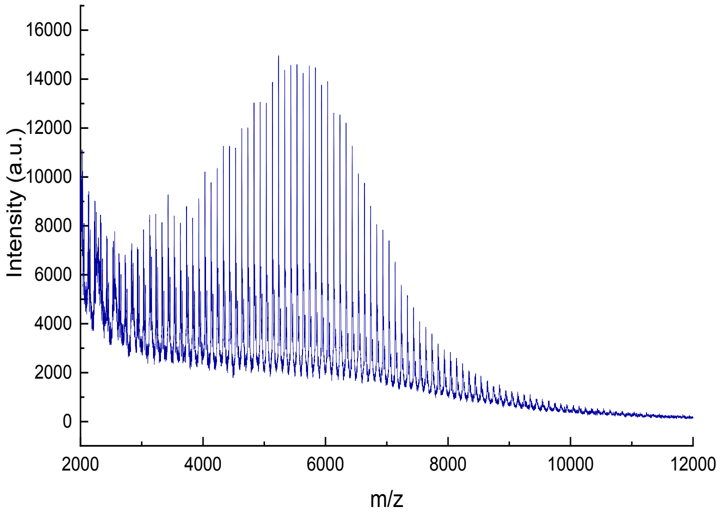

**Figure S21**. MALDI-ToF mass spectrum for polyvalerolactone (run 4).

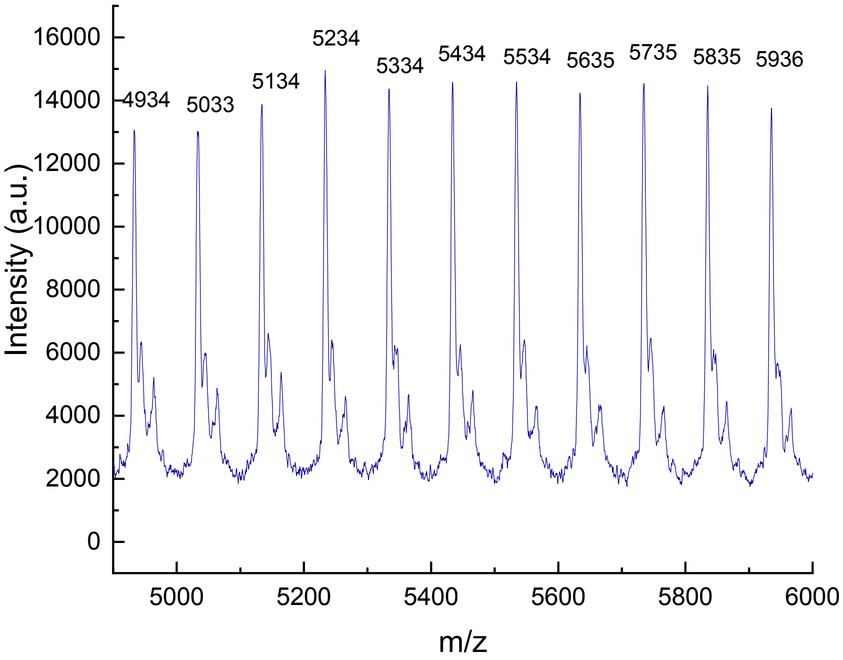

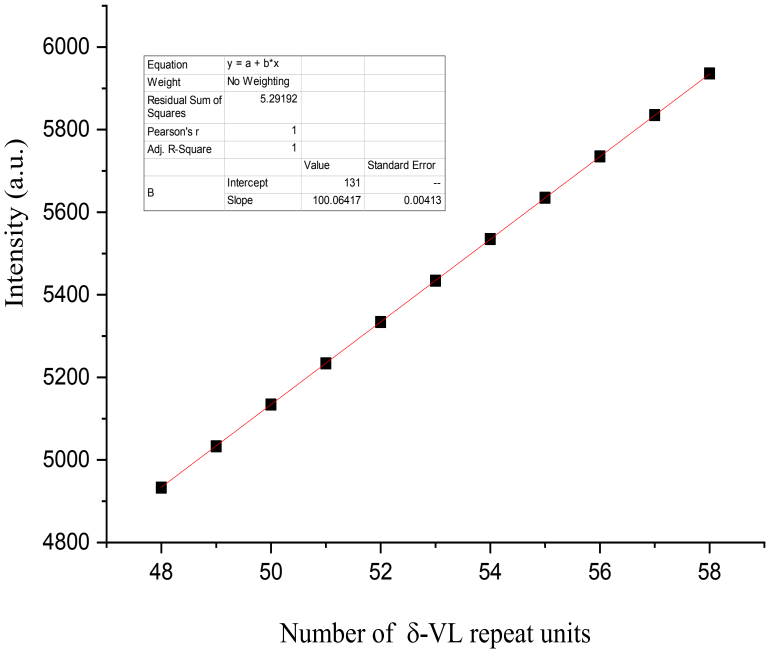

| Equation | y = a + b*x | | |
|---|---|---|---|
| Weight | No Weighting | | |
| Residual Sum of Squares | 5.29192 | | |
| Pearson's r | 1 | | |
| Adj. R-Square | 1 | | |
| | | Value | Standard Error |
| B | Intercept | 131 | -- |
| | Slope | 100.06417 | 0.00413 |

**Figure S22**. *$M_w$ vs* number of δ-VL repeat units (n) afforded a straight line with a slope of 100.6 and an intercept of 131; the slope corresponds to the exact mass of the δ-VL monomer, whereas the intercept corresponds to a polymer chain structure with benzyloxy chain-ends plus $Na^+$ (δ-VL run 4).

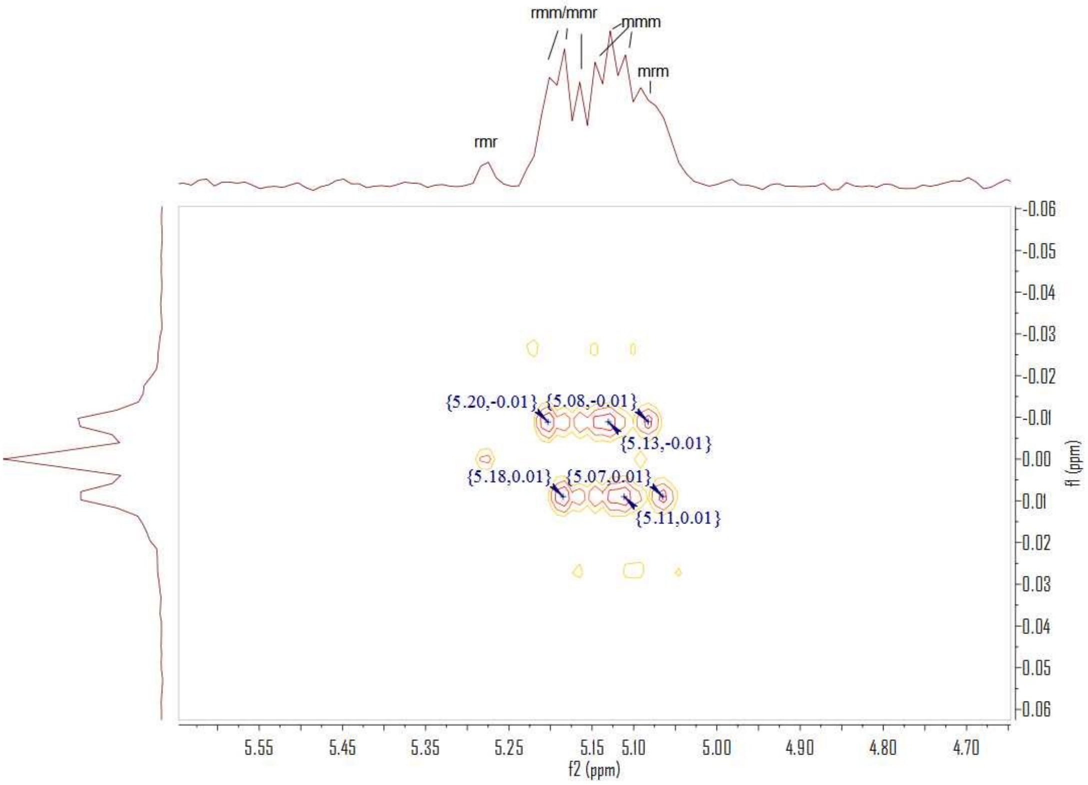

**Figure S23**. 2D J-Resolved $^1H$ NMR spectrum for co-poly (δ-VL+*r*-LA) (run 7).

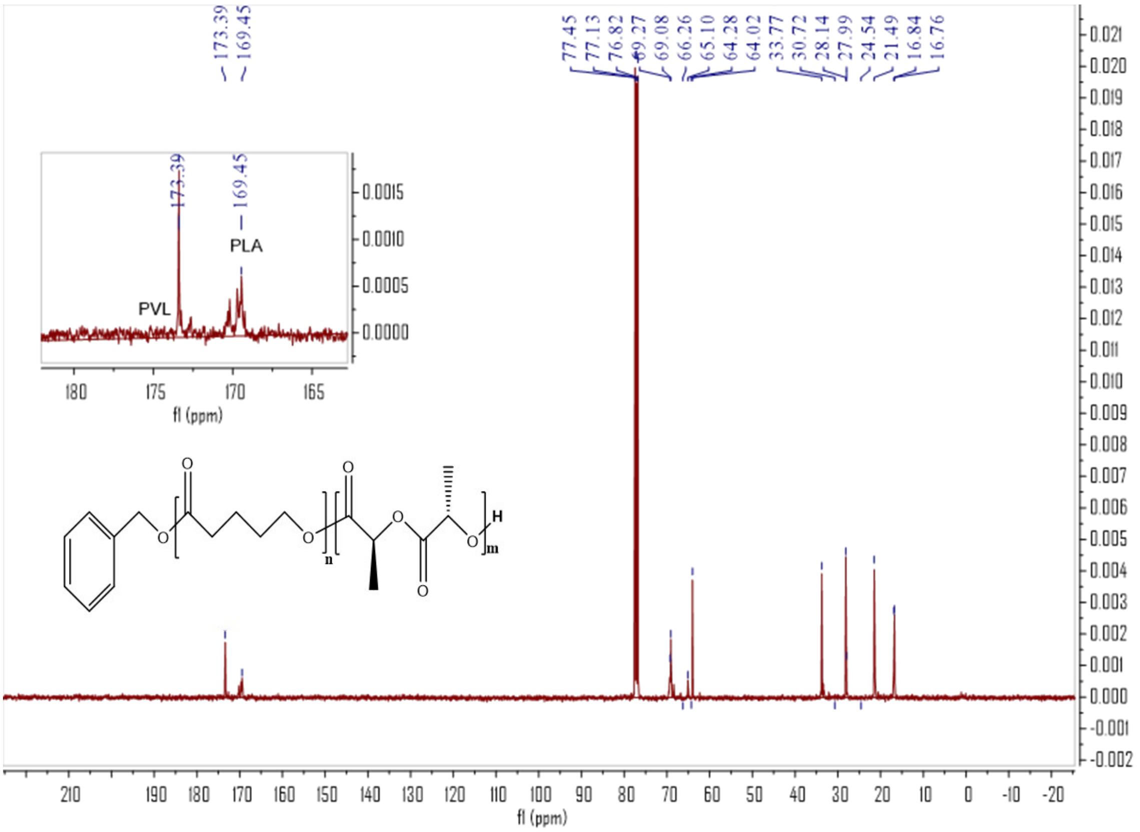

**Figure S24**.$^1$H NMR spectrum for co-poly (δ-VL+*r*-LA) (run 7).

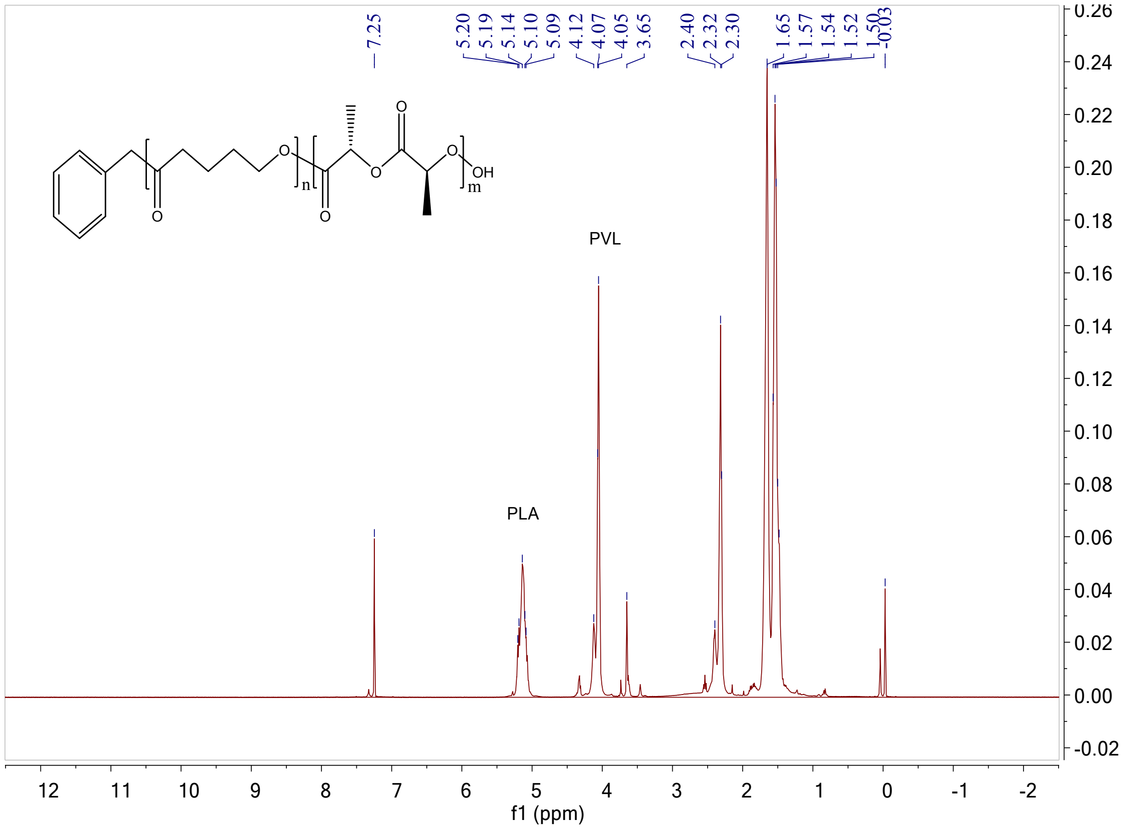

**Figure S25**. $^{13}$C NMR spectrum for co-poly (δ-VL+*r*-LA) (run 7).

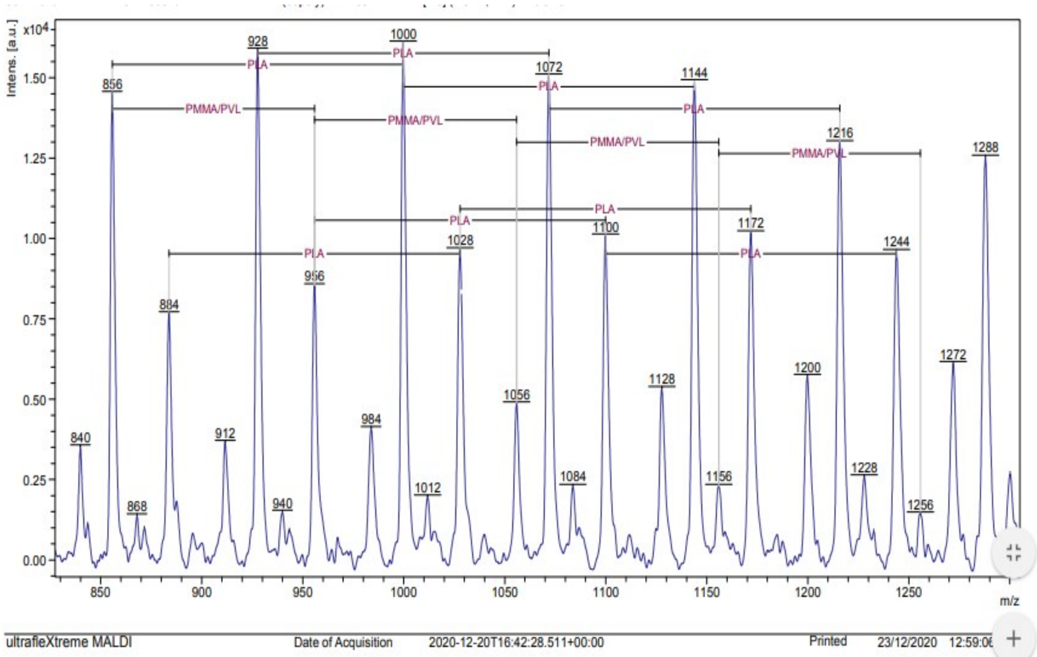

**Figure S26**. MALDI-ToF mass spectrum for co-poly (δ-VL+*r*-LA) (run 7).